



Article

Polyatomic Ion-Induced Electron Emission (IIEE) in Electrospray Thrusters

Jared M. Magnusson [†], Adam L. Collins [†] and Richard E. Wirz ^{*,†}

Plasma & Space Propulsion Laboratory, UCLA Mechanical and Aerospace Engineering, 420 Westwood Plaza, Los Angeles, CA 90095, USA; jmagnumson@ucla.edu (J.M.M.); collinsalc55@ucla.edu (A.L.C.)

* Correspondence: wirz@ucla.edu

† Current address: UCLA Department of Mechanical and Aerospace Engineering, 420 Westwood Plaza, Los Angeles, CA 90095, USA.

Received: 1 September 2020; Accepted: 21 October 2020; Published: 24 October 2020



Abstract: To better characterize the lifetime and performance of electrospray thrusters, electron emission due to electrode impingement by the propellant cation 1-ethyl-3-methylimidazolium (EMI^+) has been evaluated with semi-empirical modeling techniques. Results demonstrate that electron emission due to grid impingement by EMI^+ cations becomes significant once EMI^+ attains a threshold velocity of $\sim 9 \times 10^5 \text{ cm s}^{-1}$. The mean secondary electron yield, $\bar{\gamma}$, exhibits strong linearity with respect to EMI^+ velocity for typical electrospray operating regimes, and we present a simple linear fit equation corresponding to thruster potentials greater than 1 kV. The model chosen for our analysis was shown to be the most appropriate for molecular ion bombardments and is a useful tool in estimating IIEE yields in electrospray devices for molecular ion masses less than $\sim 1000 \text{ u}$ and velocities greater than $\sim 10^6 \text{ cm s}^{-1}$. Droplet-induced electron emission (DIEE) in electrospray thrusters was considered by treating a droplet as a macro-ion, with low charge-to-mass ratio, impacting a solid surface. This approach appears to oversimplify back-spray phenomena, meaning a more complex analysis is required. While semi-empirical models of IIEE, and the decades of solid state theory they are based upon, represent an invaluable advance in understanding secondary electron emission in electrospray devices, further progress would be gained by investigating the complex surfaces the electrodes acquire over their lifetimes and considering other possible emission processes.

Keywords: electrospray; lifetime; overspray; secondary electron emission; facility effects; kinetic emission; polyatomic ion; molecule; droplet

1. Introduction

Electrospray technology has found applicability in mass spectrometry [1], nanotechnology [2], and as a high precision attitude control thruster [3]. An electrospray emitter accelerates a conductive liquid jet under an applied electric potential. Ions are evaporated [4], and droplets can be electrostatically emitted from the jet and repelled to form a spray mixture of ions and smaller droplets. With thrust in the order of micronewtons, electrospray thrusters are well suited for CubeSat propulsion and attitude control in small satellites [3]. The Colloid MicroNewton Thruster (CMNT) developed for the European Space Agency's (ESA) Laser Interferometer Space Antenna (LISA) Pathfinder mission [5] is just one recent application exhibiting electrospray capabilities as a high specific impulse propulsion unit. With the LISA mission requiring a lifetime in excess of 60,000 hours, understanding even the most minute electrospray physics is imperative to meeting life requirements.

The Electrospray Life Model (ELM) [6,7] developed by the Plasma and Space Propulsion Laboratory (PSPL) at University of California, Los Angeles (UCLA) demonstrated [5] that thruster

lifetime can be severely compromised due to propellant over-spray and off-axis emission, resulting in undesirable impingement of the plume on the extractor and accelerator grids of the thruster assembly (Figure 1). Such impingement leads to propellant accumulation [8], which in the presence of a strong electrostatic field diminishes efficiency and causes more serious failures, such as shorting. While particular attention has been paid to propellant back-spray [7], secondary electron generation due to grid impingement may also contribute to decreased thruster lifetime [9]. Current density measurement errors can become excessive due to the stochastic generation of electrons from grid surfaces and the beam dump by ion, and perhaps even droplet bombardment [10]. In addition, electron emission due to predominantly ion bombardment becomes increasingly significant in thruster configurations without an accelerator grid where the angular current distribution is wide [11], causing increased electron emission from chamber surfaces unless suppressive measures are taken. Such electrons could also back-stream through the plume towards the emitter, neutralizing, fragmenting, and otherwise disrupting the beam profile or instigating decomposition chemistry at the emitter [6,7]. Secondary electrons generated from even low-energy ion bombardment can still accelerate to significant velocities in an electric field and eject additional electrons from chamber surfaces (tertiaries). Operating thrusters in the purely ionic regime (PIR), which occurs at high potentials, exacerbates facility effects and the quantity of electrons ejected from the beam dump. As electro spray thrusters continue seeking prolonged lifetime applications, such as the LISA mission, more attention must be paid to understanding and mitigating secondary currents from device surfaces.

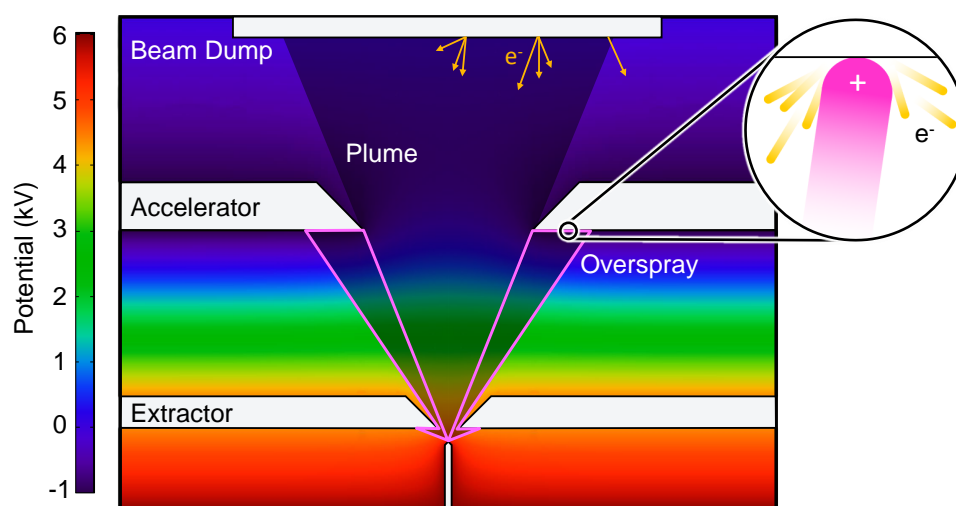


Figure 1. Electro spray thruster schematic with extraction and acceleration potentials shown (modified from [7]). Charged droplets and ions impinging the electrodes and beam dump, as shown, can cause ion-induced electron emission (IIEE), increased measurement uncertainty, and possible electron back flow.

Ion-induced electron emission (IIEE) has held research prominence for over 100 years. Numerous publications have come from the motivation to detect large macro-molecular impacts in mass spectrometry, especially as particle detection becomes challenging at low-collisional velocities [12–15]. Other applications where electron emission is critical include cosmic dust detection in space [16] and plasma material interactions (PMI) in both plasma-based thrusters and fusion reactors [17–20]. Electro spray thrusters typically employ high conductivity ionic liquids (IL) such as 1-ethyl-3-methylimidazolium bis(trifluoromethylsulfonyl)imide (EMI–Im) and 1-ethyl-3-methylimidazolium tetrafluoroborate (EMI–BF₄), both of which possess the same cation (EMI⁺). Beam particles that impinge on the grids can be a mixture of molecular ions and

droplets, depending on flow rate, applied potential, emitter geometry, propellant, and even temperature [4,21–23]. Impinging projectiles are termed primaries and all electrons emitted from the collision (both from the projectile and target surface) can be termed secondaries. Measured primary and secondary currents determine the electron emission yield, γ , defined as the ratio between the emitted electron current density and the impinging ion current density. Secondary ion emission can also result from particle impacts and may not be negligible in thruster lifetime estimates, its yield depending greatly upon surface conditions [24,25]. However, given the already large scope and differing physics of IIEE as well as the high detection efficiency of secondary ions [25], secondary ion emission will not be treated in this study, and γ will refer exclusively to secondary electron yield.

Directly studying the electron emission found in electrospray devices remains challenging because the secondaries that emerge from the grid surfaces or beam dump can be generated under substantially different and changing conditions during normal operation than from those generated in a highly-controlled experiment. Furthermore, even when substantial IIEE due to facility effects are accounted for in an experiment, observed electron yields can be higher than anticipated [26]. Reliable IIEE measurements from controlled metallic surfaces have typically required both ion-etching and annealing in an ultra-high vacuum (UHV) environment [27–30] due to the substantial complexity of surfaces generally at the atomic scale. A “technical” stainless steel surface, or a surface not cleaned in UHV conditions [24], typical of electrospray electrodes instead possesses, for example, surface oxides, chemical deposits, and asperities, to name a few complications. Furthermore, as impingement continues a thin film of propellant can accumulate on the grid’s surface, substantially altering the subsequent secondary emission. Complexities such as these render a full quantum treatment of IIEE intractable and ground state theories (e.g., density-functional theory) insufficient for such a perturbed system [31]. While IIEE theory has been developed over many decades, a full understanding of threshold emission, even for ideal metallic surfaces, remains elusive for molecular ion impacts [32,33].

To initiate discussion of secondary currents and advance electrospray thruster control-volume-type analyses without prohibitive complexity, a flat polycrystalline metal surface of zero porosity being impacted by polyatomic EMI^+ will be investigated in the context of contemporary IIEE theory. To begin, the dominant emission mechanisms must be determined, which are functions of projectile velocity and consequently the thruster’s applied potential. The threshold velocity, or the velocity at which electron emission becomes greater than zero, can then be calculated. Secondary effects will also be examined to evaluate their contributions to measured currents. These results will be analyzed and extended to see what predictions can be made for droplet impacts, if any. The objective of this paper is to determine the dominant IIEE mechanisms as well as the secondary electron yield coefficients of EMI^+ striking an electrospray thruster grid as a function of projectile energy.

2. Ion-Induced Electron Emission Mechanisms

IIEE is traditionally split into two independent mechanisms: potential electron emission (PE or PEE) and kinetic electron emission (KE or KEE). In addition, secondary effects (e.g., angle of projectile incidence or surface temperature) can manifest in non-negligible ways. After a thorough assessment of many possible IIEE processes, we found that the specific effects of PE, image-charge acceleration, thermal spikes, and surface-temperature can be reasonably ignored under typical electrospray device conditions. In addition, normal incidence on a polycrystalline surface is assumed for all projectile impacts here. These assumptions, and the justifications for them, are detailed in Appendix A should they prove pertinent to future studies. It is worth reemphasizing that IIEE can and does occur across a broad range of physical conditions and is not limited to electrospray applications. Moreover, investigation of secondary currents in other thruster types or even at other electrospray operating conditions may necessitate the inclusion of such effects as those listed in Appendix A. Thus, to examine the physics we expect to be most involved with polyatomic ion bombardment of an electrode, a general overview and evaluation of KE is now given.

KE occurs due to direct energy loss of the impacting ion with a target surface or collector. KE for high-velocity monatomic species can be broken up into a three-step process.

First, electrons are excited as the ion penetrates and interacts with the solid lattice. A comprehensive list of possible excitation mechanisms can be found in [29,34], but the dominant mechanisms are the excitation of conduction electrons into free states, the ionization of inner electron shells of the target, and ionization of the projectile itself. The energy loss of the projectile per unit depth as it traverses the medium is known as the stopping power, or dE/dx . Nuclear stopping power represents the loss of energy to target atoms through inelastic collision (Figure 2). Heavier ions can transfer sufficient momentum to an atom, so as to cause it to recoil and ionize additional atoms; the perpetuation of this process is called a recoil cascade. Energy lost by the projectile to target electrons through Coulombic interactions is called the electronic stopping power (Figure 2). While nuclear stopping power theory is relatively well-defined today, electronic stopping power computations from first principles persist as a rigorous undertaking [35]. Electronic stopping power remains of great interest for IIEE because it has been historically observed to possess the same energy dependence as electron yield [36,37].

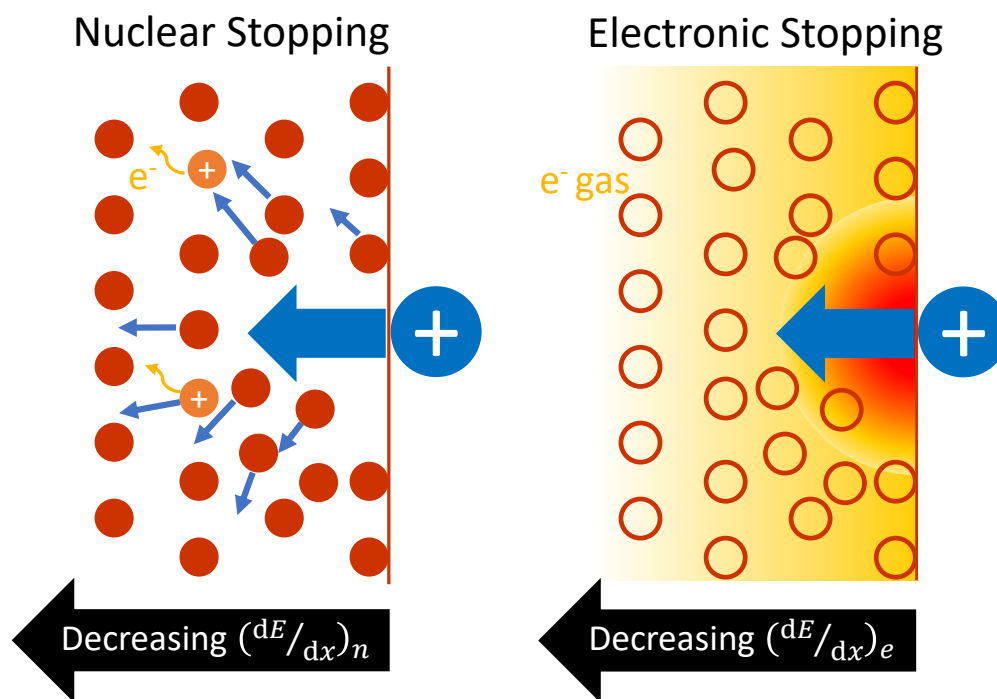


Figure 2. Nuclear and electronic stopping power as a projectile ion penetrates a metallic solid.

Second, electrons excited in the bulk must diffuse to the target surface. Typical semi-empirical models employ an electron mean-free path of around 10 \AA for metal targets [38–40] and secondary electrons energies are far too low to allow for electron escape from depths more than two to three times this value [39]. Thus, treatment of the solid as a free electron gas is acceptable for the target bulk. The simplification of a constant mean-free path has persisted in surface collision modeling and been shown to give good agreement with experimental results [38,39]. This then leads to the third step, the departure of excited electrons from the surface into the vacuum. The diffused electron's energy must exceed the surface barrier of the solid, as stated in Appendix A.1.

The three step KE process must now be adapted for low-energy, polyatomic impact on metals. At such low-velocities, molecules and clusters remain intact [34] and penetrate only the first few layers of the target. Simply put, emission begins to resemble a one-step process [41] as no significant electron scattering in the bulk occurs, so electron excitation and transmission from the surface cannot

be distinguished. In addition, the presence and thickness of an oxide will determine whether the emission surface should be treated as a conductor at all. Furthermore, because the nuclear cross-section of the target atoms increases at low projectile speeds, diverting more projectile energy into atomic collisions, the number of ionization events during penetration is no longer proportional to ion impact energy [32]. However, these atomic recoil cascades increase the importance of recoil ionization to electron yield estimates, and for heavy particle bombardment the recoil atom's velocity may even exceed that of the ion [42]. In contrast, electron cascades and multiplication may be neglected due to insufficient first-generation electron energies [41]. The complexities which arise from low energy projectile impingement limit the utility of simplified analyses and provide substantial challenges to theoretical advancements in this niche sub-discipline.

3. Materials and Methods

As discussed in Section 1, this study focuses on electron emission from EMI^+ ions, which have the empirical formula $\text{C}_6\text{H}_{11}\text{N}_2$ and a mass of 111 u. In thruster applications, EMI^+ is typically accelerated under a 2–10 kV potential [5] to reach velocities in the order of 10^6 cm s^{-1} , at or below the classical secondary electron emission threshold velocity [30]. A similar analysis to the present study could be performed for dimers or trimers of EMI^+ , as these species often have a non-negligible contribution to the beam composition (though their susceptibility to fragmentation can be high) [43,44]. Cationic monomers were chosen as a starting point to both obtain key results and more thoroughly validate chosen methods, as data for cationic surface impacts are more available in the literature. Additional analyses of anionic monomers, as well as dimers and trimers of both polarities, are topics for future study.

From the previous discussion on IIEE mechanisms per Section 2 and Appendix A, KE is the dominant emission source and our model neglects the following: PE, image-charge acceleration, thermal spikes, temperature, surface lattice orientation, porosity, and angle of incidence. As theoretical treatment of KE can be quite extensive, a complete derivation of these published models is omitted, but a brief discussion of each will be made alongside their governing assumptions.

3.1. SRIM Software

IIEE has been linked with stopping power in nearly all quantitative analyses. The calculation of stopping power, or particle energy loss to the solid per unit depth traveled, requires knowledge of the particle's velocity during penetration. For light, relativistic particles at speeds above the Bohr velocity (the velocity of an electron bound to a hydrogen atom [45]), the Bethe–Bloch theory can very accurately calculate the associated stopping powers [46,47]. For lower velocity impacts, Lindhard–Scharff–Schjøtt (LSS) stopping theory is the most relevant theoretical approach to explain radiative emission phenomena [47]. “The Stopping and Range of Ions in Matter”, or SRIM, is a computational program encompassing both Bethe–Bloch and LSS theories, providing stochastic analyses of ion trajectories in both 2-D and 3-D through a medium [47,48]. SRIM is divided into two subprograms. First is a quicker “Stopping and Range Tables” (SRT) subprogram, which computes surface stopping powers and ion ranges in many solids. The other is the “Transport of Ions in Matter” (TRIM) subprogram. TRIM offers additional support for 3-D particle tracking, stopping power as a function of particle depth, recoil losses, sputtering, and phonons. An extensive library is available for hundreds of targets with options for material layering and mixing.

Stopping power estimates using SRIM for light, high velocity ions are accurate to within 2% of experimental results, while the accuracy for slow, heavy ion stopping power calculations is better than 10% [47]. A sample of both electronic and nuclear stopping powers computed with the SRT is given in Figure 3 for the constituent atoms of EMI^+ on both copper and stainless steel.

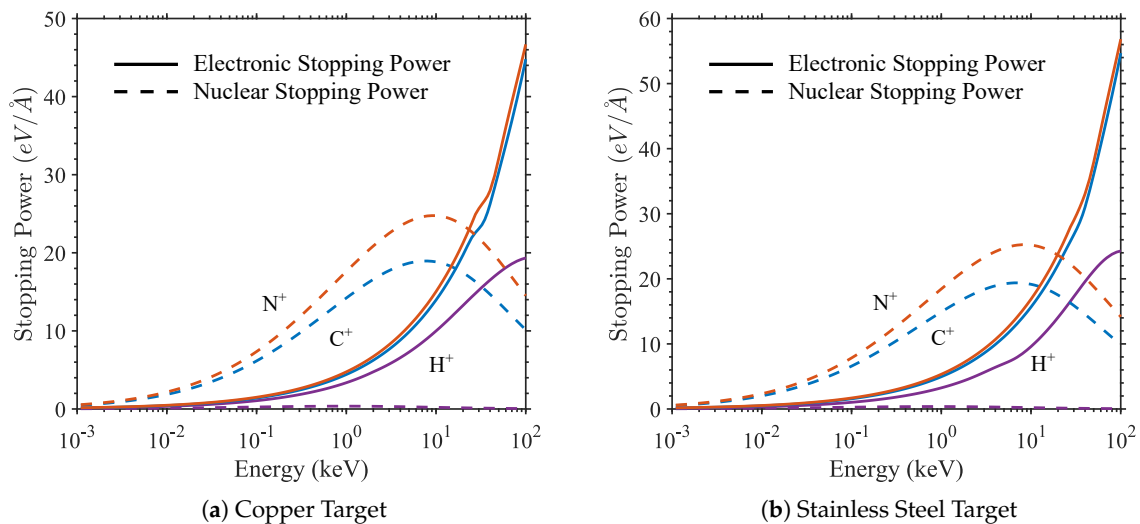


Figure 3. Surface electronic and nuclear stopping powers as a function of impact energy for H^+ , C^+ , and N^+ ions. Values were obtained with SRIM [48].

3.2. Beuhler and Friedman's First Model (Simple)

Beuhler and Friedman pioneered polyatomic IIEE modeling efforts. Their models were based on the assumption that the average electron yield from a molecular impact was equal to the sum of the average electron yields from that molecule's constituent atoms. With reference to molecular IIEE, this concept is generally referred to as "additivity" and reflects the linear mass dependence of γ seen in many experiments [14,49,50]. Both this and the following model by B&F were based upon additivity, described mathematically as

$$\bar{\gamma}_m = \sum_{atoms} \bar{\gamma}_a \quad (1)$$

where γ_m is molecular yield and γ_a is atomic yield. B&F's first model [51], which will be called the Simple model here, was based upon empirical measurements and is given by

$$\bar{\gamma}_m = \frac{1}{v_{exp} - v_{th}} \sum_{atoms} \bar{\gamma}_{a,exp} \left(\sqrt{\frac{2q_a\phi}{m_a}} - v_{th} \right) \quad (2)$$

where ϕ is the acceleration potential, q_a/m_a is the charge-to-mass ratio of each atomic species, and both v_{th} and v_{exp} are the threshold and measured velocities of $4.4 \times 10^6 \text{ cm s}^{-1}$ and $4.17 \times 10^7 \text{ cm s}^{-1}$, respectively. Noting the strong linearity seen between electron yield and velocity, average atomic yields $\bar{\gamma}_{a,exp}$ were measured at only one velocity v_{exp} and the threshold velocity v_{th} was calculated from extrapolation of their data. A copper dynode was used in their study, the limitation being that this model cannot be easily extended to other surfaces without prior measurement of $\bar{\gamma}_{a,exp}$. The Simple model was used for verification of later models discussed in this paper.

3.3. Beuhler and Friedman's Second Model (B&F)

Beuhler and Friedman's second, more rigorous theoretical treatment of molecular IIEE is given in [38]. While Equation (1) is again leveraged to obtain $\bar{\gamma}_m$, $\bar{\gamma}_a$ is correlated to the stopping power of the constituent atomic ion penetrating the target with velocity equal to that of the entire molecule—viz:

$$\bar{\gamma}_a = \frac{P}{E_0} \int_0^\infty \exp\left(-\frac{x \cos \theta}{\lambda}\right) \left(\frac{dE}{dx}\right)_e dx, \quad (3)$$

where P is the probability of electron escape from the surface to vacuum, E_0 is the average energy needed to excite an electron to escape the surface, x is the distance traveled by projectile through the solid, θ is angle between the projectile direction vector and the surface normal, λ is the characteristic wavelength of electron diffusion through the solid (i.e., the mean-free path of the excited electrons), and $(dE/dx)_e$ is the electronic stopping power. The exponential term in Equation (3) constitutes the probability of electron diffusion to the surface, and $x \cos \theta$ is the minimum distance of the projectile from the surface. With electron mean-free paths in the order of 10 \AA for metals, the importance of excitation to surface calculations at depths much greater than 30 \AA is minimal.

The electronic stopping power term $(dE/dx)_e$ represents the projectile's energy loss due to target electron excitation per unit depth traveled. Its semi-empirical formula per LSS theory is [38,52]

$$\left(\frac{dE}{dx}\right)_e = k_e \frac{8\pi e^2 a_0}{v_0} N_0 \zeta \frac{Z_1 Z_2 v}{(Z_1^{2/3} + Z_2^{2/3})^{3/2}} \quad (4)$$

where k_e is the Coulomb constant, e is elementary charge, a_0 and v_0 are the Bohr radius and Bohr velocity, respectively, N_0 is the target atomic number density, ζ is a dimensionless constant, v is the projectile velocity, and Z is the atomic number. Subscripts 1 and 2 indicate values corresponding to the projectile and target, respectively. As the electronic stopping power exhibits a linear dependence with projectile velocity and the projectile velocity depends on total (electronic and nuclear) stopping power, both penetration depth and particle velocity were solved iteratively to conserve energy per [38]. The B&F model assumes the projectile travels through the target in a straight line with no secondary losses.

Several modifications were made to the B&F model for the present study. To evaluate surfaces such as steel, a particle's electron excitation of a compound medium can be estimated (with error, see [47,48]) by assuming the yield was a weighted average of the yield in atomic surfaces. Specifically,

$$\bar{\gamma}_c = \sum_{elements} n_e \bar{\gamma}_e, \quad (5)$$

where n_e is the atomic fraction of a given element in the compound target c , with γ_c and γ_e being electron yields from the compound and elemental targets, respectively. This assumption would be identical to the Bragg–Kleeman rule [53] except that for the low energies of interest here, the stopping term cannot be brought out from the integral in Equation (3) (i.e., ion stopping power is not constant over the electron-producing regions of the target). Next, the empirical adjustments B&F made to values for ζ for atomic impacts were replaced with a more universal expression $Z_1^{1/6}$, as previously assumed [52]. Similarly, values for P and E_0 were returned to the values estimated by Sternglass [39] of 0.5 and 25 eV, respectively. As B&F reduced the value of P/E_0 by a factor of two, a $1/2$ term was added back into the B&F model, which had been introduced by Sternglass to account for energy equipartition to close collisions between δ -rays (fast, forward moving electrons) and electrons deep in the solid. Finally, assuming normal-incidence projectiles, Equation (3) becomes

$$\bar{\gamma}_a = \frac{P}{2E_0} \int_0^\infty \exp\left(-\frac{x}{\lambda}\right) \left(\frac{dE}{dx}\right)_e dx. \quad (6)$$

The form of this equation is identical to the one proposed later for fast projectiles by Baragiola et al. [30].

3.4. TRIM Model

Significant adjustments to the stopping power estimates of the B&F model were then made with SRIM. The solution form for the total yield follows that of Equations (1) and (6), except that the penetration depth and corresponding electronic stopping powers are derived from TRIM EXYZ output file data, which tabulates discrete ion stopping energies as the ion passes through the solid.

TRIM computations of stopping power take into account that the ion does not travel in a straight line but is subject to scattering. Atomic yields as a function of velocity were then fit to either arc-tangent functions following the solution forms of Axelsson et al. [12] or, in the case of proton yields, a fourth-order polynomial. Figure 4 highlights the disparity between these more recent stopping power simulations and those available to Beuhler and Friedman [38]. While electron yield comes from excitation near the surface and stopping powers need only agree for the first ~ 30 Å, the differences in Figure 4 appear drastic for all depths and will receive further discussion in Section 5. In comparing the nuclear stopping powers, one immediately notes the velocity independence assumed by Beuhler and Friedman. The slight agreement for nuclear stopping power near the surface is merely fortuitous, as SRIM values taken at different impact energies may not agree with this constant value. Furthermore, the difference in electronic stopping powers is wide even at initial penetration.

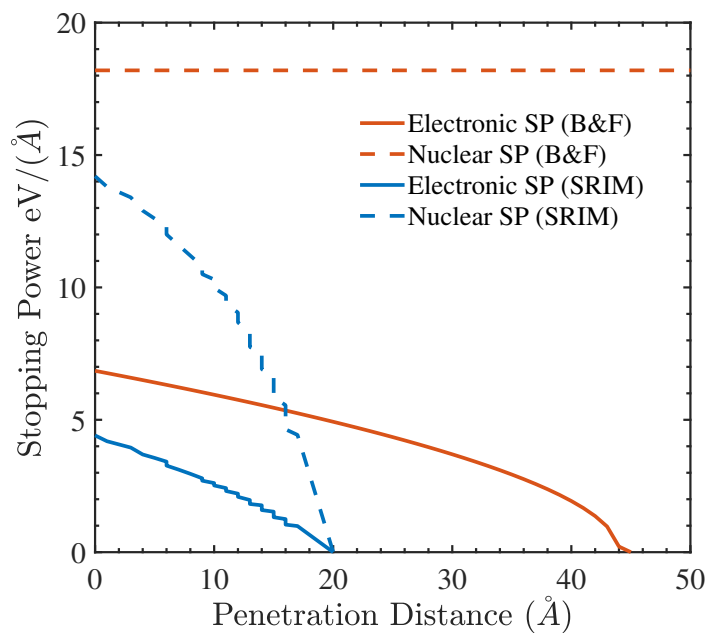


Figure 4. Stopping power of a 6 keV carbon ion as a function of penetration distance in a copper target. Calculations by Beuhler and Friedman [38] assumed no scattering. SRIM values are estimated from the SRT subprogram.

To reduce statistical errors due to the TRIM software's random number assignment when calculating particle directions, ion stopping simulations were run 100 times for every atomic ion at every energy to ensure the resulting electronic stopping powers were accurate. To exemplify the need for such averaging to the reader, over 1000 TRIM simulations were run to compute electronic stopping power as a function of nitrogen ion penetration depth in solid copper over multiple energies (Figure 5). Yields were then computed using Equation (6) per the TRIM model. Distributions were heavily skewed at high energies, but as N^+ ion energies approached those found in constituent nitrogen atoms of EMI^+ , the range shrunk significantly. Electron yield values using the simpler B&F model were always within the interquartile range (IQR) of the corresponding TRIM model distribution for the energies of interest here. Thus, the energy lost by a high-speed particle moving in a straight-line, as assumed by [38], appears to be a good approximation for TRIM calculations, which compute stochastic particle paths. This agreement will be discussed more in Section 5.

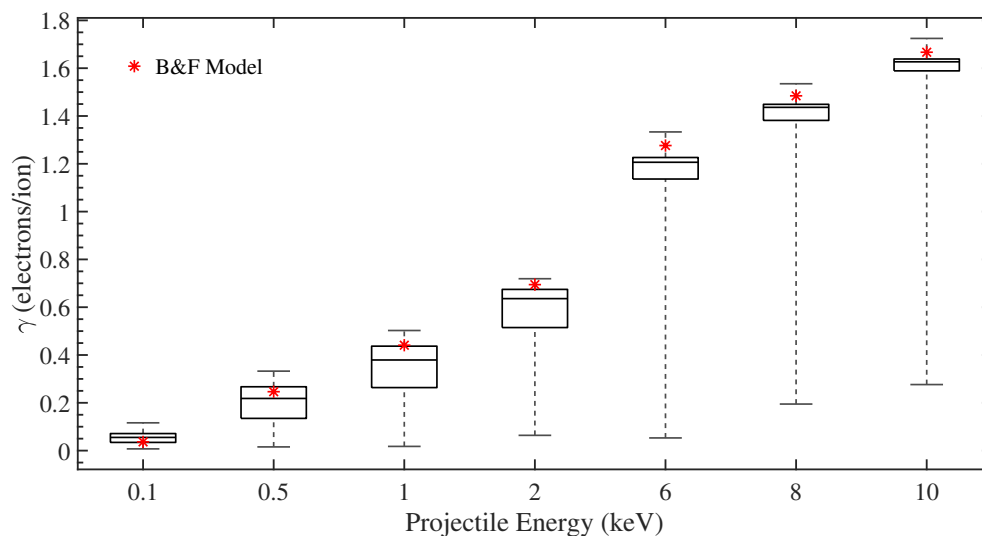


Figure 5. Box plots of TRIM model ion-induced electron yield distributions as a function of energy for nitrogen ions impacting copper. Yield calculations using the B&F model, which assume no ion scattering, are also given at each energy. Outliers are included within the whiskers for clarity.

3.5. Schou Model

Schou's theory [54] differs greatly from previous semi-empirical models. While it gives an analytical, closed solution with inputs similar to that of the B&F model, it remains the only theory accounting for cascade processes, particularly recoil ionization [29,55]. An adapted solution form for this study is as follows:

$$\bar{\gamma}_a = \Lambda \left(\beta_0 \sum_{atoms} \frac{dE}{dx_e}(x=0) + \beta_r \frac{\eta_t(\mu E)}{\mu E} \sum_{atoms} \frac{dE}{dx_n}(x=0) \right) \quad (7)$$

where Λ is a material constant, $\sum_{atoms} dE/dx$ is the additive stopping power for both electronic and collisional losses as before, β_r and β_0 account for atomic and electronic recoil transport phenomena, respectively, and η_t is a zeroth order moment of the energy distribution whose full treatment is given in [56]. The term μ (changed from γ in [56] for clarity) represents the efficiency of energy transfer in a binary collision such that μE is the maximum energy transfer possible between species. In short, the first and second terms of Equation (7) represent the spatial energy distributions transferred to target electrons due to both projectile and recoiling atom collisions, respectively. As Schou's theory provides no treatment of molecular impacts, surface stopping powers in Equation (7) were assumed additive according to the Bragg–Kleeman rule [53]. However, all other parameters are not additive. Recognizing that both the B&F and TRIM models lacked any deliberation on intramolecular dynamics, EMI^+ was assumed to be a single, heavy atom with a weighted atomic number, as any energy that may be gained or lost from molecular dissociation (~ 10 eV) upon impact is expected to be orders of magnitude lower than the kinetic energy of the impinging molecule [57].

The material constant Λ , as presented by Schou, is difficult to compute analytically, relying on stopping powers for low-energy electrons, whose energy loss functions are far from certain for calculations just above the target's Fermi energy [58,59]. Thus, the most viable technique is to determine Λ empirically by dividing γ_a by the total energy distribution into the target per Equation (7). Many previous studies on IIEE have utilized this technique. The material constant for copper used here was $0.0786 \text{ \AA eV}^{-1}$. This was averaged from two values taken at low energies by Baragiola et al. [30] and Holmén et al. [60] and reported by Hasselkamp et al. [61]. Both sources prepared surfaces meticulously in UHV chambers capable of achieving the 10^{-10} torr necessary for reproducible yield

measurements [29]. Hasselkamp et al. also reported $\Lambda = 0.1 \text{ \AA eV}^{-1}$ as an average for clean metals and semi-conductors. This was the value used for the following results involving stainless steel.

The unitless constant β_0 was set equal to 1 due to low specific projectile energies found here, in accordance with [54]. Further treatment of all other parameters follows Schou's published research.

4. Results

Validation and verification (V&V) of these semi-empirical models against relevant data are necessary before they should be applied to EMI^+ with confidence. In addition, as additivity was assumed for all models, results had to be validated for atomic as well as molecular yields. V&V also aided in seeing whether modeling results diverged for lighter, faster ions; slower, larger clusters; or both. In Figure 6, atomic yields for carbon and hydrogen ions on copper between the Schou and TRIM models are computed and compared. To the authors' knowledge, low energy data for carbon ions on copper are not available, but several sources exist for proton impacts [60–62]. Agreement between the Schou and TRIM models was good for both carbon and hydrogen ions. Overall, results adequately served to verify the models before computing molecular yields.

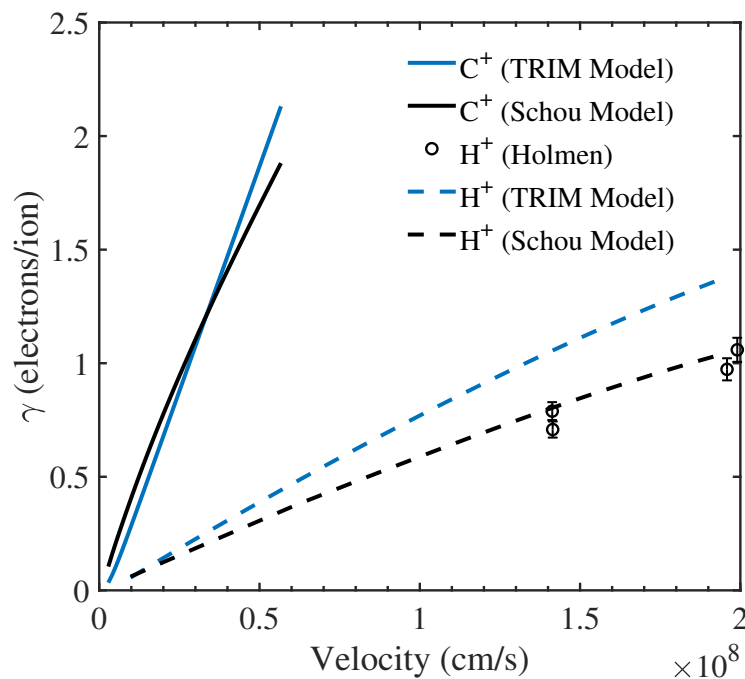


Figure 6. Average electron yield as a function of velocity for both carbon and hydrogen ions hitting copper from 0–20 keV for the TRIM and Schou models. Dashed lines represent proton impacts, while solid lines represent carbon ion impacts. Colors indicate the model utilized. Data taken from Holmén et al. (Holmen) [60].

Predicted and measured data for molecular and heavy cluster ions from previous publications were then plotted per Figure 7. Validation was split into two groups, molecules greater and less than 1000 u. Conveniently, lighter particles travelled in excess of 10^7 cm s^{-1} (approximately the classical threshold velocity of IIEE on metals) [30] while heavier particles were below this threshold. In Figure 7a, light cluster data were extracted from [15,51]. Qualitative agreement and linear velocity-dependence for all four data sets are readily noted, with the lighter carbon-based molecular yields off by a constant bias. The Schou model predicts water cluster data very well. Modeling results under-predicted data by $\sim 10\text{--}20\%$ for $\text{C}_{10}\text{F}_{17}^+$ and $\sim 30\text{--}40\%$ for $\text{C}_7\text{H}_{16}^+$.

For heavier polyatomic impacts with masses in excess of 1000 u, the most relevant measurements were again taken from singly-ionized water cluster data [50] and compared with TRIM model predictions in Figure 7b. The Schou model was not utilized because the model's general assumptions for electron excitation were not applicable for these near-droplet impacts. Data for lighter clusters ($n = 320, 500$) agreed best with the TRIM model, with modeling results increasingly over-predicting yield for heavier clusters. Disparities appear to be correlated with the mass.

Overall, the TRIM model performed best at estimating IIEE for projectiles with masses up to 10,000 u and velocities $v > 10^6$ cm s⁻¹ in Figure 7. In particular, TRIM agreed strongly with the Schou model and data for C₁₀F₁₇⁺ ions, which had mass and velocity ranges not atypical of electrospray thruster operating regimes. Therefore, it is expected that results for EMI⁺ should follow those of the TRIM model best.

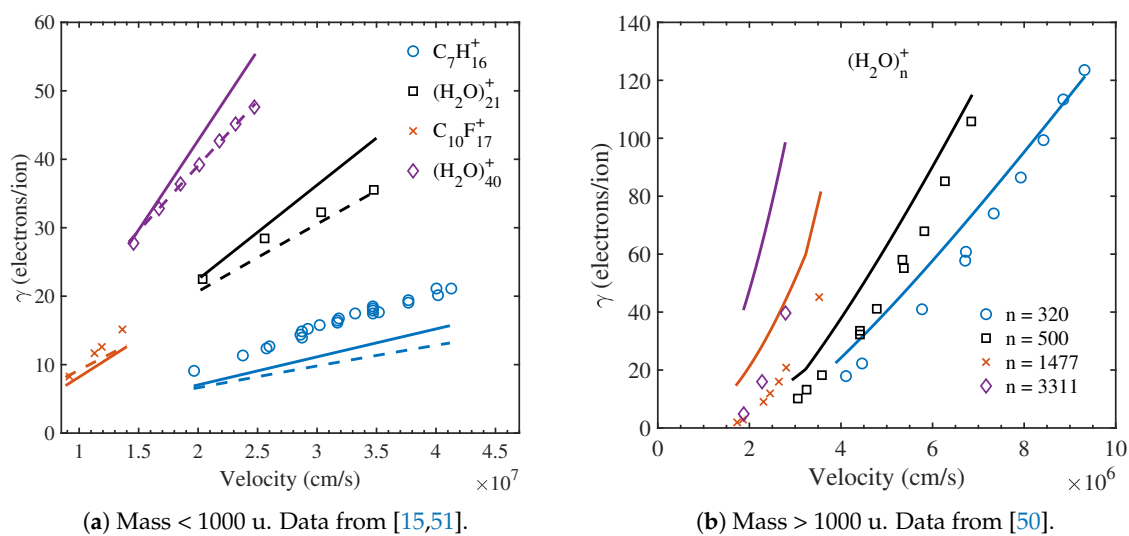


Figure 7. IIEE data as a function of velocity for molecular ions and ion clusters at 18–260 keV on copper. Solid lines are TRIM model predictions and dashed lines are predictions from the Schou model with line colors matching the corresponding data.

Finally, predicted yields for EMI⁺ on copper and stainless steel are shown in Figure 8 for all models. Particle energies of 0.05–15 keV were evaluated, which correspond to impingement velocities of 9.32×10^5 – 1.61×10^7 cm s⁻¹. Each model was applied to serve as verification in the absence of raw data. The Simple model was not applied for stainless steel, as atomic yields were not given for that surface in [51]. Good agreement is seen between the TRIM and Schou models, though their difference widens at lower projectile energies. Fit models derived empirically by Nguyen and Wien [63] are displayed for comparison to highlight possible electron yield variability due to surface conditions. It should be noted that Nguyen and Wien ion-etched their compound converters (which can lead to preferential sputtering [28]) and recorded no heat treatment of the converters to alleviate ion implantation after ion-etching. Nguyen and Wien's elevated yields for ion-etched rather than uncleaned copper in Figure 8a could stem from this approach.

Simple estimates are well-suited to control-volume analyses and other engineering applications, so curve fits may be applied to the TRIM model for typical electrospray thruster ion velocities. Again, IIEE yield curves can be well-fit with an arctangent function [12] and the results are shown in Figure 9. The fit equation is given by

$$\bar{\gamma}_{EMI} = \begin{cases} Av \tan^{-1}(B(v - v_{th})) & \text{if } v > v_{th} \\ 0 & \text{if } v \leq v_{th} \end{cases} \quad (8)$$

where $A = 3.11 \times 10^{-7}$, $B = 2.05 \times 10^{-7}$, and $v_{th} = 9.22 \times 10^5 \text{ cm s}^{-1}$ for EMI^+ . Further simplification can be made leveraging the linear velocity dependence of Equation (8) for most of its range. As electro spray thrusters have onset voltages greater than 1 kV, TRIM model data for EMI^+ can be fit to the equation (see Figure 9)

$$\bar{\gamma}_{EMI} = Cv - D, \tag{9}$$

where $C = 4.61 \times 10^{-7}$, $D = 1.19$, and v is again in cm s^{-1} . Equation (9) predicts yields within 5% of Equation (8) for ion impact energies in excess of 1 keV. IIEE yields do not exceed 1 electron/ion until EMI^+ reaches a velocity of $4.75 \times 10^6 \text{ cm s}^{-1}$ (or a corresponding energy of 1.32 keV).

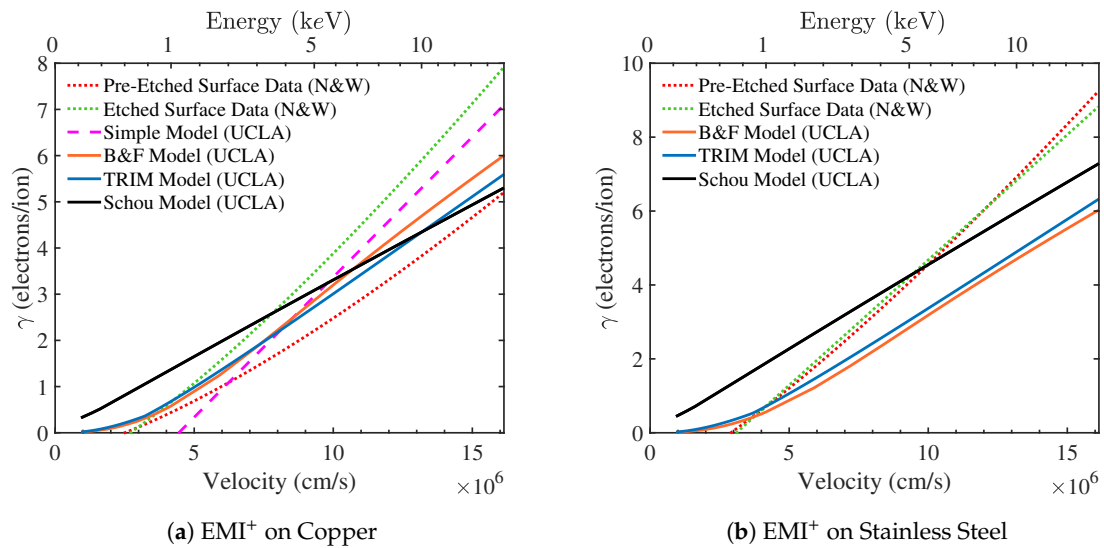


Figure 8. Electron yield for EMI^+ ions as a function of impact velocity, corresponding to impact energies of 0.05–15 keV. References for the original models are as follows: Simple model [51], B&F and TRIM models [38], and Schou model [54]. Data come from fit models derived empirically by Nguyen and Wien (N&W) [63].

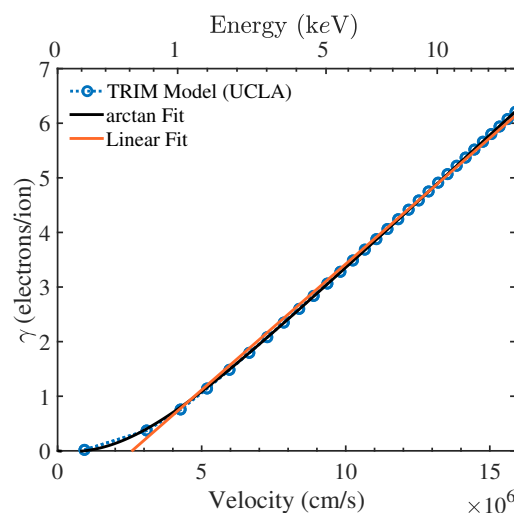


Figure 9. Average electron yield equations as a function of velocity for EMI^+ ions hitting stainless steel from 0.05–15 keV based on results from the TRIM model. The arc-tangent and linear fits are taken from Equations (8) and (9), respectively.

5. Discussion

The B&F model was an important first step in determining and validating electron yield by molecular impact. The prediction of a higher than linear order velocity dependence, which it displayed near the threshold value, has been well corroborated [12,63–65]. The TRIM model as proposed is an update of the B&F model to account for adjustments to stopping power calculations and reduce dependence on empirical measurements with what are now considered poorly-defined surfaces [29,30]. However, both the B&F and TRIM models oversimplify the physics manifested during secondary emission. The B&F model's ability to match empirical data is limited by its ill-defined input parameters (e.g., P , E_0 , and ζ ; see [30]), and adjustments by Beuhler and Friedman to these constants reflect this. Furthermore, TRIM and B&F models' assumption of additivity implies molecular breakup. Calculating the total yield from the penetration and electron excitation of a molecule's individual atoms insinuates that the molecule would traverse the target just as deeply as its constituent atoms at the same velocity.

The results of Figure 6 serve as a necessary validation of atomic yields to be used in the TRIM model. Agreement between the Schou and TRIM models is excellent for carbon impacts, but less so for hydrogen. However, component hydrogen energies in a large molecule such as EMI^+ here will be much lower than even 1 keV, where the Schou and TRIM models agree more strongly.

Strong similarity between the B&F and TRIM models is seen in Figure 8, which would appear straightforward except that the stopping powers used to compute yields varied significantly per Figure 4. There are multiple reasons for the agreement. First, electron stopping powers are not so drastically different as depicted in Figure 4 at energies lower than 1 keV, and differences in penetration distance after 25–30 Å grow increasingly unimportant, as few electrons will make it to the surface from such depths. Nevertheless, Figure 4 demonstrates higher electronic stopping powers for the B&F model. One could argue that the TRIM model's electron yields match those of the B&F model so well because its lower electronic stopping power values are compensated by increased ion scattering in the near-surface regions of the target. Median TRIM model nitrogen ion yields were less than those predicted by the B&F model at every energy except 0.1 keV, which is the more appropriate energy for EMI^+ 's constituent nitrogen atoms for many thruster modes. Indeed, the TRIM model predicted an average γ_a over 30% higher than that predicted by the B&F model at 0.1 keV, illustrating that ion scattering does indeed play a role in low energy IIEE. As projectile energies increase, the projectile undergoes fewer atomic collisions in the near-surface regions of the solid and its path there begins to resemble that of a straight-line. Disagreement between the TRIM and B&F models decreases with increasing energy, and for 10 keV nitrogen ions the difference does not exceed 2.5%. Simply put, inelastic collisions increasingly deflect the particle at decreasing energies such that it will not travel in a straight line as assumed in the B&F model. This leads to a greater quantity of electron escape as the ion stays closer to the surface for a greater proportion of its penetration distance, compensating for perceived differences in stopping power observed in a single dimension.

On the other hand, the Schou model makes no assumption as to the penetration distance of the projectile, a relatively uncertain variable for low energy calculations. Surface stopping power values are all that is required in Equation (7). It is also the only theory which takes recoiling atom ionization into account, which is an important phenomenon because electrospray devices operate at the low energies shown in Figure 3. Moreover, Schou's theory has been strongly validated with experimental results and is simply a superior treatment of the underlying physics involved [29]. However, difficulties arise with application of the Schou model to polyatomic impacts, and its solution for EMI^+ should be treated with caution. Schou noted breakdown of his theory at low energies, where the assumption of a cascade ionization no longer holds well [54,55]. Departure from assumed conditions was seen when applying the Schou model to cluster impacts with velocities less than 10^7 cm s^{-1} , which is again near the classical velocity threshold for IIEE. In addition, parameters such as β_r , η_t , and μ are not additive and had to be solved for by assuming the projectile acted as a single, heavy atom with a weighted

atomic number. Furthermore, total yield values remain highly sensitive to the material parameter Λ , which must yet be determined empirically.

Figure 7a furthers the discussion of model accuracy. Both 1000 u and 10^7 cm s⁻¹ have been used as previous limits for investigating the additivity of molecular yield [63]. Thus, we cannot necessarily expect accurate results from the TRIM model for all projectile energies. The TRIM model yield results disagreed with fast impact data for C₇H₁₆⁺ and C₁₀F₁₇⁺ by ~10–40%, though this is not unexpected given that the test chamber pressure in [51] was four orders of magnitude higher than recommended vacuum conditions for an already inadequately-prepared surface [29]. Thus, even significantly different empirical results for γ can be expected unless surfaces are prepared to a level comparable to the model's assumptions [30]. The TRIM model also disagreed with the data for (H₂O)₂₁⁺ and (H₂O)₄₀⁺ because additivity of electron yield for light water clusters was not observed per the original analysis [15]. However, given the Schou model's excellent reproduction of this supposedly non-additive result, one would expect it to be due to superior testing conditions, though this does not appear to be so [50]. Overall, first-order estimates of heavy, intermediate velocity impacts are adequately obtained using both the TRIM and Schou models.

Figure 7b underscores a lower velocity limit to these models. Sensible results were only obtained with the TRIM model, which diverged increasingly from water cluster yields with increasing mass. Nevertheless, results for the $n = 320$ and 500 clusters were acceptable, and the original authors reported additivity for the $n = 320$ cluster [50]. These heavy-cluster results may depict a different mechanism for electron emission that is not well represented by KE. The threshold velocity classically derived for metals [30] is over an order of magnitude higher than the threshold velocities depicted in Figure 7b, Figure 8, and additionally predicted by Equation (8), though our threshold velocity for EMI⁺ matches those of similar molecules quite well [15,64]. At such low impact velocities, electron excitation becomes a surface, rather than bulk, phenomenon. Thus, the free electron-gas model as defined from bulk parameters, a fundamental assumption, is not necessarily relevant and experimental validation requires near perfect control of surface conditions [64]. IIEE theorists and experimentalists agree that a quasi-molecular auto-ionization is responsible for emission below 10^7 cm s⁻¹ due to large electron cloud overlap [16,41,66], though thorough investigation into the underlying theory remains in progress. Other studies of the sub-classical emission threshold argue that IIEE enhancements stem from projectile excitation [67], bulk and surface plasmon decay [68], and electron cascades induced by Auger transitions [69]. Thus, these verifiable results for EMI⁺ cations may exceed experimental yields by a factor of two as reported for the heavy water clusters in Figure 7b, as both operate in similar velocity regimes. Isolation of KE from secondary processes is therefore imperative. Recent work has demonstrated the ability to separate KE and PE contributions to electron emission utilizing grazing incidence projectiles on well prepared surfaces [70]. A more advanced computational theory including secondary processes is also necessary for comparison. Unfortunately, the experimental work surrounding IIEE greatly surpasses the theory [33].

As molecular clusters grow and even exceed 50,000 u, results begin to approach droplet induced electron emission (DIEE). Secondaries due to possible ion evaporation from the droplet surface have been seen in colloid thrusters [10]. However, typical charge-to-mass ratios for EMI–Im [71] droplets are so low that DIEE may be completely irrelevant [72]. Characterization of DIEE, if any occurs, will out of necessity rely on the parameterization of direct measurements for now, similar to that done by [63] except that the impact velocities of such droplets would be in the order of 10^4 cm s⁻¹ (far below observed IIEE threshold velocities). Unexpected environmental factors may further complicate DIEE. For example, while droplet splashing on a dry surface in vacuum is impossible [73], splashing can occur on the thin liquid films atop a propellant-saturated surface [74–76]. Initial experiments should vary inputs with care, as tests on an oxidized electrode with deliberate accumulation are so uncharacteristic of historic IIEE studies.

Electrospray thruster grids can be designed with a conductive porous foam material in order to absorb accumulated propellant and improve thruster lifetime [5]. While the theory behind

surface permeability effects on electron yield are underway in the context of sputtering [77] and electron-induced electron emission (SEE) [19,78,79], corresponding theoretical treatments for IIEE have only recently begun [20]. The authors were unable to find studies of IIEE due to molecular ions impacting a porous metallic foam. Furthermore, semi-empirical models calculating sputtering and SEE yields from a porous surface are often functions of impermeable or “flat” yield measurements [77,79], and the latter are also unknown for polyatomic ion impacts of interest here. Thus, verifiable estimates must be obtained for impermeable substrates first before surface porosity effects can be discussed. Moreover, as porous surfaces offer significant reductions in yield over flat surfaces [19,20,77], values obtained in this work represent an upper bound for electron yields expected in a functional electro-spray device using porous electrodes.

6. Conclusions

Current best estimates of IIEE from EMI^+ impacts occurring under typical electro-spray conditions have been obtained. Three semi-empirical models were considered that reflect the surface physics relevant for characterizing the life and performance of electro-spray thrusters. IIEE yields for EMI^+ have a threshold velocity of $9.22 \times 10^5 \text{ cm s}^{-1}$ and have been shown to possess a linear velocity dependence over common electro-spray thruster operating conditions per Equation (9). Mean electron yield, $\bar{\gamma}$, varies approximately linearly from one to six electrons/ion for EMI^+ velocities of 4.75×10^6 – $1.61 \times 10^7 \text{ cm s}^{-1}$ which correspond to energies of 1.3–15 keV. For velocities less than $4.75 \times 10^6 \text{ cm s}^{-1}$ (1.3 keV), $\bar{\gamma}$ has been shown to be nonlinear with velocity, and its expected profile is strongly dependent upon the governing theory assumed. Additional research is required to reduce uncertainty of IIEE yields for projectile energies below 1 keV and quantify the secondary effects which become non-negligible at lower velocities. Nevertheless, Equation (9) is an appropriate model where IIEE yields are most pronounced, and normal impacts below the energy threshold of Equation (9) are not expected to generate electron yields above one electron/ion. Thus, tests of thrusters operating in the PIR must take secondaries into account, though facility effects due to secondaries are likely to disrupt mixed emission modes as well. These results will help to both advance analyses of electro-spray thruster performance and life as well as mature control-volume analyses of charge conservation in plume-surface interaction studies.

The TRIM model, an adjustment of the equations derived by Beuhler and Friedman [38] based on more reliable stopping power estimates available today, was shown to be the most appropriate model for molecular ion bombardments and is a useful tool in estimating IIEE yields in electro-spray devices. However, as the typical operating regimes of electro-spray thrusters reside near the lower bound of IIEE theory, we recommend limiting application of the TRIM model to ion masses less than $\sim 1000 \text{ u}$ and velocities greater than $\sim 10^6 \text{ cm s}^{-1}$. We encourage future work to expand and adjust polyatomic IIEE emission theory for auto-ionization processes, projectile incidence, and porous surfaces as necessary. In the last case, electron yield measurements should be a fraction of results obtained here, and our findings will support further development of IIEE theory on uneven or permeable surfaces.

As knowledge of current transfer between the electro-spray emitter and grids evolves, more thorough analysis of other sources of charge, such as secondary ion emission and droplet-induced electron emission, can be performed. These source studies are inextricably coupled with the complex surfaces that electro-spray electrodes acquire over their lifetimes. We expect IIEE behavior on thin films to differ strongly from patterns observed in solid surface impacts. In the specific case of DIEE, the treatment of an impacting droplet as a large, minimally-charged ion is unfounded. We encourage both propulsion and surface scientists to continue research into this intricate, multifaceted field.

Author Contributions: Conceptualization, A.L.C. and R.E.W.; Data curation, J.M.M.; Formal analysis, J.M.M.; Funding acquisition, R.E.W.; Investigation, J.M.M.; Methodology, J.M.M.; Project administration, A.L.C. and R.E.W.; Resources, A.L.C. and R.E.W.; Supervision, A.L.C. and R.E.W.; Validation, J.M.M.; Visualization, J.M.M., A.L.C. and R.E.W.; Writing—original draft, J.M.M.; Writing—review and editing, J.M.M., A.L.C. and R.E.W. All authors have read and agreed to the published version of the manuscript.

Funding: This work was funded by grants from NASA/JPL award number 1580267:3 and Air Force Research Laboratory award number 16-EPA-RQ-09.

Conflicts of Interest: The authors declare no conflict of interest. The funders had no role in the design of the study; in the collection, analyses, or interpretation of data; in the writing of the manuscript, or in the decision to publish the results.

Appendix A. Additional Emission Mechanisms

Fundamental IIEE mechanisms and effects which were deemed negligible for the analysis relevant to electrospray thrusters in this study are given here. Pertinent emission sources, including kinetic emission, are presented in Section 2.

Appendix A.1. Potential Emission

PE results from an Auger process, either Auger neutralization or a combination of both resonance neutralization and Auger de-excitation [16,31,80,81]. In the case of Auger neutralization (AN), which is the more efficient electron emission mechanism of the two [16,80], an electron from the valence band of a surface tunnels a few angstroms to an electron vacancy in the projectile [81]. A valence electron from the surface is also released with a maximum kinetic energy equal to the difference between the impinging ion's potential energy E_i (first ionization energy) and twice the binding energy of the solid surface barrier (i.e., the work function (Φ) for metals or the band gap plus electron affinity for insulators) [41]. Thus, for metals, PE via AN cannot occur if the condition $E_i - 2\Phi > 0$ is unmet.

To estimate PE using fundamental ion and surface properties, Kishinevsky [82] derived a widely used equation which calculates electron yield as a function of projectile ionization energy and surface work function, viz:

$$\gamma = \frac{0.2}{\epsilon_F} (0.8E_i - 2\Phi) \quad \text{for } 3\Phi < E_i < 2(\epsilon_F + \Phi), \quad (\text{A1})$$

where ϵ_F is the target Fermi energy. Yields were also shown to saturate at values around 0.5 electrons/ion when the upper bound was exceeded. Equation (A1) was well-corroborated with a least squares fit to existing data by Baragiola et al. [30], whose results are plotted in Figure A1 for stainless steel.

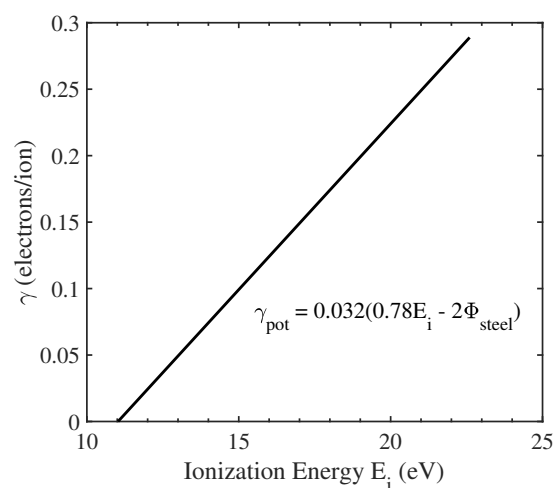


Figure A1. PE yield as a function of ionization energy for stainless steel. Steel's work function is 4.3 eV [83]. The equation shown comes from [30].

Though an exact value has not been calculated, the ionization energy for EMI^+ is very likely to be in the order of 10 eV [84]. Further, assuming any PE caused by EMI^+ is due to its component nitrogen ion with an ionization energy of about 14 eV [85] (an assumption from [86] and supported by [12]), the maximum yield of EMI^+ impacting stainless steel is expected to be less than 0.1 electrons/ion.

For a technical steel surface like an electrode, yields would be even lower, as the condition $E_i > 2\Phi$ is generally unmet in the presence of adsorbed molecules (an innate complication to electrospray devices which requires its own dedicated study) [41]. All authors studying single-valency ion impacts have noted PE's minimal importance for nearly the entire velocity regime of interest here, demonstrating that yield does not exceed a value of 1 electrons/ion [1,16,29,34,49,63,66]. If desired, further rationale as to why empirical molecular PE yields are lower than similar impacts by monatomic ions is given by Baragiola [16,32], though advanced theory behind molecule-induced PE remains undeveloped. Accordingly, contributions of PE to IIEE are irrelevant in electrospray devices considered here.

Appendix A.2. Image-Charge Acceleration

Conductive materials will develop an image-charge as charged particles approach the surface. The incoming projectile ion receives additional velocity from acceleration due to the image charge attraction until it is close enough to the surface to neutralize; the acceleration is proportional to the charge-to-mass ratio of the impinging particle [81]. More detail on the manifestation and consequences of image charge acceleration is given by Axelsson et al. [1,12]; however, for singly-charged ions and charged droplets of the charge-to-mass ratios expected for electrosprayed species [71,87], the gain in kinetic energy from said image charge acceleration does not lead to significant enhancement of either PE or KE, and is not considered further in this study.

Appendix A.3. Thermal Spikes

Thermal spikes have been heavily investigated by authors attempting to determine the mass dependence of IIEE. Results for molecular ions of energies comparable to, or even much greater than, those of EMI^+ have shown no thermal spiking effect [13,49,50]. These spikes are much more readily identified in extremely slow, heavy particle impacts, such as from cosmic dust [16]. For technical surfaces the presence of an oxide, which likely developed during the experiments in [49,50] due to oxide-friendly chamber conditions, did not render thermal spikes any more detectable. Thus, thermal spikes have been omitted from our analysis.

Appendix A.4. Surface Temperature

Generally, the temperature dependence of ion impact for conductive surfaces is agreed to be negligible, though this is not true for insulating surfaces [29]. An exception for conductive targets occurs if the surface undergoes a phase change due to annealing, where yield exhibits a step-wise increase at the annealing temperature [88]. A well-controlled experiment by Benka et al. [89] with MeV ions found a linear decrease in electron yield with temperature, though the relative change in yield per unit temperature never exceeded $1.2 \times 10^{-4} \text{ K}^{-1}$ for copper. Given that the temperature dependence of IIEE appears minimal, temperature effects are neglected for the calculations in this work.

Appendix A.5. Projectile Incidence Angle

Secondary emission has been demonstrated to be sensitive to the angle of incidence of the projectile [60,62,90]. As secondary electrons diffuse to the surface from a relatively shallow portion of the target and grazing-angle impacts lengthen the distance traveled by the projectile in that near-surface region, the number of excited electrons emitted increases with incidence angle. Electron yield increases with a secant or near-secant dependence on incidence angle for light, high-velocity ions [62]. However, secant dependencies were not seen for lower energy particles where nuclear stopping was dominant [62]. Indeed, IIEE theory lacks matured understanding of angular dependence, especially for heavy ions [54], and both experiments and semi-empirical models generally assume normal incidence [29]. Furthermore, heavy molecules penetrate only a few angstroms into the target and incidence angles are poorly defined for polycrystalline surfaces of any roughness such that high electron yield variability is expected [90]. To prevent overextending the theory, all projectile impacts

are taken at normal incidence to a polycrystalline surface in this work, though deeper understanding of incidence effects on IIEE are imperative to future development.

References

1. Axelsson, J.; Reimann, C.; Sundqvist, B. Secondary electron emission from surfaces impacted by multiply-charged polyatomic ions. *Nucl. Instrum. Methods Phys. Res. Sect. Beam Interact. Mater. Atoms* **1994**, *88*, 131–137. [[CrossRef](#)]
2. Salata, O.V. Tools of nanotechnology: Electrospray. *Curr. Nanosci.* **2005**, *1*, 25–33. [[CrossRef](#)]
3. Mier-Hicks, F.; Lozano, P.C. Electrospray thrusters as precise attitude control actuators for small satellites. *J. Guid. Control. Dyn.* **2017**, *40*, 642–649. [[CrossRef](#)]
4. Romero-Sanz, I.; Bocanegra, R.; Fernandez De La Mora, J.; Gamero-Castano, M. Source of heavy molecular ions based on Taylor cones of ionic liquids operating in the pure ion evaporation regime. *J. Appl. Phys.* **2003**, *94*, 3599–3605. [[CrossRef](#)]
5. Ziemer, J.; Marrese-Reading, C.; Dunn, C.; Romero-Wolf, A.; Cutler, C.; Javidnia, S.; Li, T.; Li, I.; Franklin, G.; Barela, P.; et al. Colloid microthruster flight performance results from space technology 7 disturbance reduction system. In Proceedings of the 35th International Electric Propulsion Conference, Atlanta, GA, USA, 8–12 October 2017; pp. 1–17.
6. Thuppul, A.; Wright, P.; Wirz, R.E. Lifetime Considerations and Estimation for Electrospray Thrusters. In Proceedings of the 2018 Joint Propulsion Conference, Cincinnati, OH, USA, 9–11 July 2018; pp. 4652:1–4652:12.
7. Thuppul, A.; Wright, P.L.; Collins, A.L.; Ziemer, J.; Wirz, R.E. Lifetime Considerations for Electrospray Thrusters. *Aerospace* **2020**, *7*, 108. [[CrossRef](#)]
8. Uchizono, N.M.; Collins, A.L.; Thuppul, A.; Wright, P.L.; Eckhardt, D.Q.; Ziemer, J.; Wirz, R.E. Emission Modes in Electrospray Thrusters Operating with High Conductivity Ionic Liquids. *Aerospace* **2020**, *7*, 141. [[CrossRef](#)]
9. Wirz, R.E. Electrospray Thruster Performance and Lifetime Investigation for the LISA Mission. In Proceedings of the AIAA Propulsion and Energy 2019 Forum, Indianapolis, IN, USA, 19–22 August 2019; pp. 3816:1–3816:27.
10. Marrese-Reading, C.; Ziemer, J.; Gamero-Castano, M.; Bame, D.; Demmons, N.; Hruby, V. Plasma Potential Measurements in the Plume of a Colloid Micro-Newton Thruster. In Proceedings of the 42nd AIAA/ASME/SAE/ASEE Joint Propulsion Conference & Exhibit, Sacramento, CA, USA, 9–12 July 2006; pp. 4642:1–4642:7.
11. Natisin, M.R.; Zamora, H.L. Performance of a Fully Conventionally Machined Liquid-Ion Electrospray Thruster Operated in PIR. In Proceedings of the 36th International Electric Propulsion Conference, Vienna, Austria, 9–12 September 2019; pp. 522:1–522:16.
12. Axelsson, J.; Parilis, E.; Reimann, C.; Sullivan, P.; Sundqvist, B. Electron emission from conducting surfaces impacted by multiply-charged polyatomic ions. *Nucl. Instrum. Methods Phys. Res. Sect. Beam Interact. Mater. Atoms* **1995**, *101*, 343–356. [[CrossRef](#)]
13. Hofer, W.O. Emission of atoms and electrons from high-density collision cascades in metals. *Nucl. Instrum. Methods* **1980**, *170*, 275–279. [[CrossRef](#)]
14. Xu, Y.; Bae, Y.; Beuhler, R.; Friedman, L. Secondary electron analysis of polymeric ions generated by an electrospray ion source. *J. Phys. Chem.* **1993**, *97*, 11883–11886. [[CrossRef](#)]
15. Beuhler, R.J. A comparison of secondary electron yields from accelerated water cluster ions ($M/z < 50,000$) striking Al_2O_3 and copper surfaces. *J. Appl. Phys.* **1983**, *54*, 4118–4126.
16. Baragiola, R.A. Electron emission from surfaces by impact of polyatomic ions and cosmic dust. *Nucl. Instrum. Methods Phys. Res. Sect. Beam Interact. Mater. Atoms* **1994**, *88*, 35–43. [[CrossRef](#)]
17. Taccogna, F.; Longo, S.; Capitelli, M. Plasma-surface interaction model with secondary electron emission effects. *Phys. Plasmas* **2004**, *11*, 1220–1228. [[CrossRef](#)]
18. Gunn, J. Evidence for strong secondary electron emission in the tokamak scrape-off layer. *Plasma Phys. Control. Fusion* **2012**, *54*, 085007:1–085007:7. [[CrossRef](#)]
19. Patino, M.; Wirz, R. Electron emission from carbon velvet due to incident xenon ions. *Appl. Phys. Lett.* **2018**, *113*, 041603:1–041603:3. [[CrossRef](#)]

20. Huerta, C.E.; Wirz, R.E. Ion-induced electron emission reduction via complex surface trapping. *AIP Adv.* **2019**, *9*, 125009:1–125009:6. [[CrossRef](#)]
21. Cloupeau, M.; Prunet-Foch, B. Electrostatic spraying of liquids in cone-jet mode. *J. Electrostat.* **1989**, *22*, 135–159. [[CrossRef](#)]
22. Juraschek, R.; Röllgen, F. Pulsation phenomena during electrospray ionization. *Int. J. Mass Spectrom.* **1998**, *177*, 1–15. [[CrossRef](#)]
23. Romero-Sanz, I.; De Carcer, I.A.; de la Mora, J.F. Ionic propulsion based on heated Taylor cones of ionic liquids. *J. Propuls. Power* **2005**, *21*, 239–242. [[CrossRef](#)]
24. Walton, S.; Tucek, J.; Champion, R.; Wang, Y. Low energy, ion-induced electron and ion emission from stainless steel: The effect of oxygen coverage and the implications for discharge modeling. *J. Appl. Phys.* **1999**, *85*, 1832–1837. [[CrossRef](#)]
25. Westmacott, G.; Ens, W.; Standing, K. Secondary ion and electron yield measurements for surfaces bombarded with large molecular ions. *Nucl. Instrum. Methods Phys. Res. Sect. Beam Interact. Mater. Atoms* **1996**, *108*, 282–289. [[CrossRef](#)]
26. Patino, M.I.; Wirz, R.E. Characterization of xenon ion and neutral interactions in a well-characterized experiment. *Phys. Plasmas* **2018**, *25*, 062108:1–062108:13. [[CrossRef](#)]
27. Musket, R.; McLean, W.; Colmenares, C.A.; Makowiecki, D.; Siekhaus, W. Preparation of atomically clean surfaces of selected elements: A review. *Appl. Surf. Sci.* **1982**, *10*, 143–207. [[CrossRef](#)]
28. Taglauer, E. Surface cleaning using sputtering. *Appl. Phys. A* **1990**, *51*, 238–251. [[CrossRef](#)]
29. Hasselkamp, D.; Rothard, H.; Groeneveld, K.O.; Kemmler, J.; Varga, P.; Winter, H. *Particle Induced Electron Emission II*; Springer: Berlin/Heidelberg, Germany, 1992; Volume 123.
30. Baragiola, R.; Alonso, E.; Ferron, J.; Oliva-Florio, A. Ion-induced electron emission from clean metals. *Surf. Sci.* **1979**, *90*, 240–255. [[CrossRef](#)]
31. Winter, H.; Burgdörfer, J. *Slow Heavy-Particle Induced Electron Emission From Solid Surfaces*; Springer: Berlin/Heidelberg, Germany, 2007; Volume 225.
32. Baragiola, R.A. Principles and mechanisms of ion induced electron emission. *Nucl. Instrum. Methods Phys. Res. Sect. Beam Interact. Mater. Atoms* **1993**, *78*, 223–238. [[CrossRef](#)]
33. Le Beyec, Y. Cluster impacts at keV and MeV energies: Secondary emission phenomena. *Int. J. Mass Spectrom. Ion Process.* **1998**, *174*, 101–117. [[CrossRef](#)]
34. Fallavier, M. Secondary electron emission of solids by impact of molecular ions and clusters. *Nucl. Instrum. Methods Phys. Res. Sect. Beam Interact. Mater. Atoms* **1996**, *112*, 72–78. [[CrossRef](#)]
35. Correa, A.A. Calculating electronic stopping power in materials from first principles. *Comput. Mater. Sci.* **2018**, *150*, 291–303. [[CrossRef](#)]
36. Bethe, H.A. On the theory of secondary emission. *Phys. Rev.* **1941**, *59*, 940–949.
37. Massey, H.S.W.; Burhop, E.H.S. *Electronic and Ionic Impact Phenomena*; Clarendon Press: Oxford, UK, 1952.
38. Beuhler, R.; Friedman, L. A model of secondary electron yields from atomic and polyatomic ion impacts on copper and tungsten surfaces based upon stopping-power calculations. *J. Appl. Phys.* **1977**, *48*, 3928–3936. [[CrossRef](#)]
39. Sternglass, E. Theory of secondary electron emission by high-speed ions. *Phys. Rev.* **1957**, *108*, 1–12. [[CrossRef](#)]
40. Parilis, E.; Kishinevskii, L. The Theory of Ion-Electron Emission. *Sov. Phys. Solid State* **1960**, *3*, 885.
41. Baragiola, R.; Riccardi, P. Electron emission from surfaces induced by slow ions and atoms. In *Reactive Sputter Deposition*; Springer: Berlin/Heidelberg, Germany, 2008; pp. 43–60.
42. Ferron, J.; Alonso, E.V.; Baragiola, R.A.; Oliva-Florio, A. Electron emission from molybdenum under ion bombardment. *J. Phys. Appl. Phys.* **1981**, *14*, 1707–1720. [[CrossRef](#)]
43. Courtney, D.G.; Dandavino, S.; Shea, H. Comparing direct and indirect thrust measurements from passively fed ionic electrospray thrusters. *J. Propuls. Power* **2016**, *32*, 392–407. [[CrossRef](#)]
44. Mehta, N.A.; Levin, D.A. Molecular dynamics electrospray simulations of coarse-grained ethylammonium nitrate (EAN) and 1-ethyl-3-methylimidazolium tetrafluoroborate (EMIM-BF₄). *Aerospace* **2018**, *5*, 1. [[CrossRef](#)]
45. Bohr, N. *The Penetration of Atomic Particles Through Matter*; Matematisk-fysiske Meddelelser: Munksgaard København; Det Kongelige Danske Videnskabernes Selskab: Copenhagen, Denmark, 1948; Volume XVIII(8), p. 38.

46. Ziegler, J. Stopping of energetic light ions in elemental matter. *J. Appl. Phys.* **1999**, *85*, 1249–1272. [[CrossRef](#)]
47. Ziegler, J.F.; Biersack, J.P.; Ziegler, M.D. *SRIM—The Stopping and Range of Ions in Matter*; SRIM Co.: Rimini, Italy, 2008.
48. Ziegler, J.F.; Biersack, J.P. *SRIM—The Stopping and Range of Ions in Matter*; Version 2013.00. 2013. Available online: <http://www.srim.org> (accessed on 20 August 2020).
49. Thum, F.; Hofer, W.O. No enhanced electron emission from high-density atomic collision cascades in metals. *Surf. Sci.* **1979**, *90*, 331–338. [[CrossRef](#)]
50. Beuhler, R.; Friedman, L. Threshold studies of secondary electron emission induced by macro-ion impact on solid surfaces. *Nucl. Instrum. Methods* **1980**, *170*, 309–315. [[CrossRef](#)]
51. Beuhler, R.; Friedman, L. Low noise, high voltage secondary emission ion detector for polyatomic ions. *Int. J. Mass Spectrom. Ion Phys.* **1977**, *23*, 81–97. [[CrossRef](#)]
52. Lindhard, J.; Scharff, M.; Schiøtt, H.E. Range concepts and heavy ion ranges (Notes on Atomic Collisions, II). *Mat. Fys. Medd. K. Dan. Vidensk. Selsk.* **1963**, *33*, 1–42.
53. Bragg, W.H.; Kleeman, R. XXXIX. On the α Particles of Radium, and Their Loss of Range in Passing Through Various Atoms and Molecules. *Lond. Edinb. Dublin Philos. Mag. J. Sci.* **1905**, *10*, 318–340. [[CrossRef](#)]
54. Schou, J. Transport theory for kinetic emission of secondary electrons from solids. *Phys. Rev. B* **1980**, *22*, 2141–2174. [[CrossRef](#)]
55. Sigmund, P.; Tougaard, S. Electron emission from solids during ion bombardment. Theoretical aspects. In *Inelastic Particle-Surface Collisions*; Springer: Berlin/Heidelberg, Germany, 1981; pp. 2–37.
56. Holmén, G.; Svensson, B.; Schou, J.; Sigmund, P. Direct and recoil-induced electron emission from ion-bombarded solids. *Phys. Rev. B* **1979**, *20*, 2247–2254. [[CrossRef](#)]
57. Luo, Y.R.; *Comprehensive Handbook of Chemical Bond Energies*; CRC Press: Boca Raton, FL, USA, 2007.
58. Tanuma, S.; Powell, C.J.; Penn, D.R. Calculations of stopping powers of 100 eV to 30 keV electrons in 10 elemental solids. *Surf. Interface Anal.* **2005**, *37*, 978–988. [[CrossRef](#)]
59. Chantler, C.; Bourke, J. Electron inelastic mean free path theory and density functional theory resolving discrepancies for low-energy electrons in copper. *J. Phys. Chem. A* **2014**, *118*, 909–914. [[CrossRef](#)]
60. Holmén, G.; Svensson, B.; Burén, A. Ion induced electron emission from polycrystalline copper. *Nucl. Instrum. Methods Phys. Res.* **1981**, *185*, 523–532. [[CrossRef](#)]
61. Hasselkamp, D.; Hippler, S.; Scharmann, A.; Schmehl, T. Electron emission from clean solid surfaces by fast ions. *Ann. Phys.* **1990**, *502*, 555–567. [[CrossRef](#)]
62. Svensson, B.; Holmen, G.; Burén, A. Angular dependence of the ion-induced secondary-electron yield from solids. *Phys. Rev. B* **1981**, *24*, 3749–3755. [[CrossRef](#)]
63. Nguyen, V.; Wien, K. Secondary electron emission from various metals and CsI bombarded by heavy molecular ions. *Nucl. Instrum. Methods Phys. Res. Sect. Beam Interact. Mater. Atoms* **1998**, *145*, 332–345. [[CrossRef](#)]
64. Brunelle, A.; Chaurand, P.; Della-Negra, S.; Le Beyec, Y.; Parilis, E. Secondary electron emission yields from a CsI surface under impacts of large molecules at low velocities (5×10^3 – 7×10^4 ms⁻¹). *Rapid Commun. Mass Spectrom.* **1997**, *11*, 353–362. [[CrossRef](#)]
65. Hasselkamp, D.; Lang, K.; Scharmann, A.; Stiller, N. Ion induced electron emission from metal surfaces. *Nucl. Instrum. Methods* **1981**, *180*, 349–356. [[CrossRef](#)]
66. Lakits, G.; Aumayr, F.; Heim, M.; Winter, H. Threshold of ion-induced kinetic electron emission from a clean metal surface. *Phys. Rev. A* **1990**, *42*, 5780–5783. [[CrossRef](#)] [[PubMed](#)]
67. Zampieri, G.; Meier, F.; Baragiola, R. Formation of autoionizing states of Ne in collisions with surfaces. *Phys. Rev. A* **1984**, *29*, 116–122. [[CrossRef](#)]
68. Baragiola, R.A.; Dukes, C.A. Plasmon-assisted electron emission from Al and Mg surfaces by slow ions. *Phys. Rev. Lett.* **1996**, *76*, 2547–2550. [[CrossRef](#)]
69. Minniti, M.; Commisso, M.; Sindona, A.; Barone, P.; Bonanno, A.; Oliva, A.; Riccardi, P. The role of Al-Auger electrons in kinetic electron emission from Al surfaces by slow Ne⁺ and Na⁺ ions. *Nucl. Instrum. Methods Phys. Res. Sect. Beam Interact. Mater. Atoms* **2007**, *257*, 618–622. [[CrossRef](#)]
70. Winter, H.; Lederer, S.; Aumayr, F.; Winter, H. Electron emission for grazing slow atom and ion impact on monocrystalline metal and insulator surfaces. *Phys. Scr.* **2005**, *72*, C12–C21. [[CrossRef](#)]
71. Gamero-Castaño, M. The structure of electrospray beams in vacuum. *J. Fluid Mech.* **2008**, *604*, 339–368. [[CrossRef](#)]

72. Gamero-Castano, M.; Fernandez De La Mora, J. Direct measurement of ion evaporation kinetics from electrified liquid surfaces. *J. Chem. Phys.* **2000**, *113*, 815–832. [[CrossRef](#)]
73. Guo, Y.; Lian, Y.; Sussman, M. Investigation of drop impact on dry and wet surfaces with consideration of surrounding air. *Phys. Fluids* **2016**, *28*, 073303:1–073303:24. [[CrossRef](#)]
74. Yarin, A.; Weiss, D. Impact of drops on solid surfaces: self-similar capillary waves, and splashing as a new type of kinematic discontinuity. *J. Fluid Mech.* **1995**, *283*, 141–173. [[CrossRef](#)]
75. Cossali, G.; Coghe, A.; Marengo, M. The impact of a single drop on a wetted solid surface. *Exp. Fluids* **1997**, *22*, 463–472. [[CrossRef](#)]
76. Josserand, C.; Zaleski, S. Droplet splashing on a thin liquid film. *Phys. Fluids* **2003**, *15*, 1650–1657. [[CrossRef](#)]
77. Li, G. Plasma Sputtering Behavior of Structured Materials. Ph.D. Thesis, University of California, Los Angeles, CA, USA, 2020.
78. Huerta, C.; Patino, M.; Wirz, R. Secondary electron emission from textured surfaces. *J. Phys. D Appl. Phys.* **2018**, *51*, 145202:1–145202:8. [[CrossRef](#)]
79. Swanson, C.; Kaganovich, I.D. Modeling of reduced effective secondary electron emission yield from a velvet surface. *J. Appl. Phys.* **2016**, *120*, 213302:1–213302:9. [[CrossRef](#)]
80. Hagstrum, H.D. Theory of Auger ejection of electrons from metals by ions. *Phys. Rev.* **1954**, *96*, 336–365. [[CrossRef](#)]
81. Varga, P. Neutralization of multiply charged ions at a surface. *Appl. Phys. A* **1987**, *44*, 31–41. [[CrossRef](#)]
82. Kishinevsky, L. Estimation of electron potential emission yield dependence on metal and ion parameters. *Radiat. Eff.* **1973**, *19*, 23–27. [[CrossRef](#)]
83. Wilson, R. Vacuum Thermionic Work Functions of Polycrystalline Be, Ti, Cr, Fe, Ni, Cu, Pt, and Type 304 Stainless Steel. *J. Appl. Phys.* **1966**, *37*, 2261–2267. [[CrossRef](#)]
84. Seki, K. Ionization energies of free molecules and molecular solids. *Mol. Cryst. Liq. Cryst.* **1989**, *171*, 255–270. [[CrossRef](#)]
85. Lide, D.R. *CRC Handbook of Chemistry and Physics*; CRC Press: Boca Raton, FL, USA, 2004; Volume 85.
86. Lakits, G.; Winter, H. Electron emission from metal surfaces bombarded by slow neutral and ionized particles. *Nucl. Instrum. Methods Phys. Res. Sect. Beam Interact. Mater. Atoms* **1990**, *48*, 597–603. [[CrossRef](#)]
87. Lozano, P.C. Studies on the Ion-Droplet Mixed Regime in Colloid Thrusters. Ph.D. Thesis, Massachusetts Institute of Technology, Cambridge, MA, USA, 2003.
88. Andrianova, N.; Avilkina, V.; Borisov, A.; Mashkova, E.; Parilis, E. The study of graphite disordering using the temperature dependence of ion-induced electron emission. *Vacuum* **2012**, *86*, 1630–1633. [[CrossRef](#)]
89. Benka, O.; Steinbatz, M. Temperature dependence of the electron and ion induced electron emission yield of Al, Cu and Ag. *Nucl. Instrum. Methods Phys. Res. Sect. Beam Interact. Mater. Atoms* **2003**, *201*, 396–404. [[CrossRef](#)]
90. Dietz, L.; Sheffield, J. Secondary electron emission induced by 5–30-keV monatomic ions striking thin oxide films. *J. Appl. Phys.* **1975**, *46*, 4361–4370. [[CrossRef](#)]

Publisher's Note: MDPI stays neutral with regard to jurisdictional claims in published maps and institutional affiliations.



© 2020 by the authors. Licensee MDPI, Basel, Switzerland. This article is an open access article distributed under the terms and conditions of the Creative Commons Attribution (CC BY) license (<http://creativecommons.org/licenses/by/4.0/>).